

THE PROXIMITY EFFECT, THE UV BACKGROUND AND THE STATISTICS OF THE LYMAN-ALPHA LINES AT HIGH RESOLUTION ¹

E. Giallongo², S. Cristiani^{3,4}, S. D'Odorico⁴, A. Fontana², S. Savaglio^{4,5}

² Osservatorio Astronomico di Roma, via dell'Osservatorio, I-00040 Monteporzio, Italy

³ Dipartimento di Astronomia, Università di Padova, vicolo dell'Osservatorio 5, I-35122, Padova, Italy

⁴ European Southern Observatory, Karl Schwarzschild Strasse 2, D-85748 Garching, Germany

⁵ Istituto di Astrofisica Spaziale del CNR, Frascati, Italy

¹Based on observations collected at the 3.5m New Technology Telescope of ESO for the Key program 2-013-49K

Received _____; accepted _____

ABSTRACT

We present results from high resolution ($R \simeq 28000$) spectra of six high-redshift QSOs taken at the ESO NTT telescope that allow the detailed study of the Lyman- α population in the redshift interval $z = 2.8 - 4.1$.

The typical Doppler parameters found for the Lyman- α lines lie in the interval $b = 20 \div 30 \text{ km s}^{-1}$, corresponding to temperatures $T > 24000 \text{ K}$, with a fraction of the order 15% in the range $10 \leq b \leq 20 \text{ km s}^{-1}$. These values are still consistent with models of low density, highly ionized clouds.

The observed redshift and column density distributions obtained from these spectra and from the observations of 4 additional QSOs taken in the literature allow an accurate estimate of the proximity effect from a relatively large Lyman- α sample (more than 1100 lines with $\log N_{HI} \geq 13.3$) in the redshift interval $z = 1.7 - 4.1$.

A Maximum Likelihood analysis has been applied to estimate *simultaneously* the best fit parameters of the Lyman- α statistics *and* of the UV background. After correcting for the blanketing of weak lines, we confirm that the column density distribution is best represented by a double power-law with a break at $\log N_{HI} \simeq 14$, with a slope $\beta_s = 1.8$ for higher column densities and a flatter slope $\beta_f = 1.4$ below the break.

A value $J_{LL} = 5 \pm 1 \times 10^{-22} \text{ erg cm}^{-2} \text{ s}^{-1} \text{ Hz}^{-1} \text{ sr}^{-1}$ is derived for the UV background in the redshift interval $z = 1.7 - 4.1$, consistent with the predicted QSO contribution. No evidence is found for redshift evolution of the UVB in the same redshift interval.

The comoving volume density distributions of protogalactic damped systems, Lyman Limit systems and Lyman- α clouds with $\log N_{HI} \gtrsim 14$ and radii $R \simeq 200 \text{ kpc}$ are found to be similar, suggesting a possible common association with

galaxies.

1. Introduction

The statistics of the Lyman- α absorptions, seen in QSO spectra shortward of the Lyman- α emission, provide unique information about the physical and cosmological properties of the neutral gas phase of the baryonic component of the Universe. The high sensitivity of the observations of the Lyman- α lines allows to investigate very different structures, ranging from fluctuations of the diffuse intergalactic medium to the interstellar medium in protogalactic disks. This scientific driver coupled with the advances in instrumental and detector capabilities at 4-m class telescope has led in the last few years to a flourishing of investigations on Lyman- α forest (e.g. Pettini et al. 1990, Carswell et al. 1991, Rauch et al. 1993, Giallongo et al. 1993, Fan & Tytler 1994, Cristiani et al. 1995). The new data have sufficient resolution ($R > 20000$) and signal-to-noise ratio to use line-fitting procedures to obtain reliable estimate of the L- α clouds parameters like redshift, column density N_{HI} and Doppler width b and a more detailed physical picture of the absorbing gas has emerged.

The average Doppler parameter is found to be $b \lesssim 30 \text{ km s}^{-1}$, corresponding to an average temperature $T \sim 5 \times 10^4 \text{ K}$. This is typical for clouds in photoionization equilibrium with the general UV ionizing background. However, the presence of a non negligible fraction of narrow lines with $b = 10 - 20 \text{ km s}^{-1}$ has been recognized in the highest resolution spectra, although the assessment of the real fraction relies on the S/N ratio of the data and on the intrinsic blending of the lines, which is strong at very high redshifts. It is difficult to reconcile, using standard photoionization models, temperatures $T \sim 15000 - 20000 \text{ K}$ with the large cloud sizes $R \sim 50 - 150 h^{-1} \text{ kpc}$ inferred from observations of QSO pairs (Smette et al. 1992, 1995; Bechtold et al. 1994; Dinshaw et al. 1995). This has led to the introduction of particular cooling mechanisms (Giallongo & Petitjean 1994).

The Lyman- α lines show an appreciable redshift evolution in the redshift range $z = 1.7 - 4$ and small clustering, limited at $\Delta v < 300 \text{ km s}^{-1}$ for lines with $\log N_{HI} \gtrsim 13.8$

(Cristiani et al. 1995). Attempts have been done to explain these cosmological properties in the framework of the CDM cosmology (e.g. Miralda-Escudé & Rees 1994, Cen et al. 1994).

The introduction of the HIRES echelle spectrograph at the Keck 10m telescope has given new impulse to the observations. Recent spectra with HIRES have revealed the presence of CIV absorption associated with Lyman- α lines with $\log N_{HI} \gtrsim 14$ (Cowie et al. 1995, Tytler & Fan 1995). The derived abundances, although dependent on the ionization state of the Lyman- α clouds, seem to be similar to the ones derived for the heavy element absorptions originated in galaxy halos, suggesting a continuity in their physical properties.

The high resolution observations of the Lyman- α forest provide also a powerful method to estimate the UV background at high redshifts. It is already known from low resolution Lyman- α samples that the redshift evolution of the line number density, within a single spectrum, does not follow the general cosmological trend when approaching the QSO emission redshift. This “inverse effect” has been interpreted and modeled as a “proximity effect” (Weymann, Carswell, & Smith 1981; Tytler 1987; Bajtlik, Duncan & Ostriker 1988). It consists in a reduction of the line density in the region near the QSO emission redshift due to the increase of the ionizing flux by the QSO. In this way, absorbers near QSOs are more highly ionized than those farther away where the general UV background is the only source of ionization.

Using a simple photoionization model Bajtlik, Duncan, & Ostriker 1988 showed that the predicted and observed proximity effects agreed at high redshift adopting the value $J_{LL} \sim 10^{-21} \text{ erg cm}^{-2} \text{ s}^{-1} \text{ Hz}^{-1} \text{ sr}^{-1}$ for the UV background at the Lyman limit. This estimate has been confirmed within uncertainties of ± 0.5 in $\log J_{LL}$ by Lu, Wolfe & Turnshek 1991. The most comprehensive analysis of the proximity effect has been published by Bechtold 1994 on the basis of a homogeneous low resolution ($R \sim 3500$) Lyman- α sample derived from the spectra of 34 QSOs in the redshift range $1.6 < z < 4.1$. She found a value about 3 times

higher, $J_{-21} = 3$ and a correlation of the proximity effect on the QSO luminosities as expected from the photoionization model. However, any analysis performed at low resolution does not allow the use of the correct column density and redshift distributions for the Lyman- α lines, both affecting the estimate of the UV background from the proximity effect. Giallongo et al. (1993) and Cristiani et al. (1995) on the basis of a few quasars observed at high resolution ($R \gtrsim 25000$), suggest a rather flat power-law column density distribution for lines with $\log N_{HI} < 14$ and a value of the UV background sensibly smaller than the reference value $\log J_{LL} = -21$ at $z \sim 3$, even if the uncertainties were relatively large.

We discuss in this paper a larger sample including more than 1100 Lyman- α lines with column densities $\log N_{HI} \geq 13.3$, observed at an average $R \sim 25000$, and perform a Maximum Likelihood analysis to estimate *simultaneously* the parameters of the Lyman- α line distributions *and* the intensity of the UV background in the redshift interval $1.7 < z < 4.1$. In particular, in section 2.1 our data sample is defined, in section 2.2 the $b - \log N_{HI} < 14$ distribution and its implication on the temperature of the Lyman- α clouds are analysed. In section 2.3 and 2.4 we discuss the H I column density and redshift distribution respectively. Section 3 gives the details of the computation and the results on the UV background. The conclusions of our work are listed in section 4.

We adopt throughout the value $H_o = 50 \text{ km s}^{-1} \text{ Mpc}^{-1}$ for the Hubble parameter and $q_o = 0.5$.

2. Lyman- α Statistics

2.1. The Data Sample

Most of the data used in this analysis come from the ESO key programme 2-013-49K (P.I. S.D’Odorico) devoted to the study of the intergalactic medium at high redshifts. Up to

now spectra of six QSOs, at a resolution between 9 and 14 km s⁻¹, have been reduced. The list of the objects, with emission redshifts ranging from 3.3 to 4.1 is given in Table 1 together with the main characteristics of the Lyman- α absorption line sample. Spectra of the QSOs 2126-158 and 0055-269 have been already published (Giallongo et al. 1993; Cristiani et al. 1995). For 2126-158 new spectra have been added, significantly improving the S/N with respect to the published data. A complete description of the data sample will be given in a separate paper: here we focus on the main statistical properties of the Lyman- α clouds that can be derived from this sample.

All the spectra have been analyzed in a uniform way and all the lines have been fitted using our FITLYMAN program which is now available in the ESO-MIDAS package (Fontana & Ballester 1995). It performs a χ^2 minimization to derive the redshift z , the Doppler parameter b and the column density N for isolated lines and individual components of the blends. As done in previous similar analyses (e.g. Giallongo et al. 1993), complex structures with often asymmetric profiles have been fitted with the minimum number of components required to give a probability of random deviation $P > 0.05$.

To identify heavy element systems we have compared the lists of the observed lines with a list, derived from Morton 1991, containing the most frequently seen lines in QSO absorption spectra. As customary, we searched for significant excesses of identifications at all possible redshifts (Bahcall 1968). All the identified heavy element systems present in the Lyman- α forest have been removed from the final sample, which consists of more than 1100 Lyman- α lines with observed column density $\log N_{HI} \geq 13.3$. Whenever possible, the Lyman- β forest has been used to constrain the number of components in the strong saturated Lyman- α blends as shown in Fig. 1.

The S/N has been computed from the noise spectrum, and is typically greater than 10 per pixel element (corresponding to 15 per resolution element). In the regions near the QSO

Lyman- α emissions, where the proximity effect is important, and for the brighter quasars the S/N raises to higher values $\sim 15 - 40$, corresponding to S/N $\sim 20 - 60$ per resolution element. Extensive simulations by various authors (Rauch et al. 1993, Fontana & Ballester 1995) show that no strong bias in the derived statistical distributions is expected when the S/N is >10 and $\log N_{HI} > 13$.

We have complemented our data with other spectra available in the literature with similar resolution and redshift range obtaining a final sample of 10 QSOs (in the following referred to as *extended sample*), that is $\sim 30\%$ of the number of objects used by Bechtold (1994) , but observed at resolution ten times higher.

2.2. The $b - N_{HI}$ Distributions and the Temperature of the Lyman- α Clouds

The average resolution ($R \sim 25000$) of our extended sample corresponds, in terms of Voigt profile fitting, to a minimum Doppler parameter $b \simeq 7 \text{ km s}^{-1}$, which is equivalent to a temperature $T \sim 3000 \text{ K}$ and thus adequate to assess the photoionization state of the Lyman- α clouds.

If we restrict our analysis to the two objects with the best S/N ratio (20-60 per resolution element), 0000-26 and 2126-158 (Fig.2), we can obtain reliable measurements of the Doppler profiles of the weak lines down to $\log N_{HI} \lesssim 13$. In Figs. 3 and 4 we show the $b - N_{HI}$ distributions derived from 0000-26 and 2126-158 respectively, while Fig. 5 gives the histograms of the Doppler parameter.

These plots confirm the earlier result (Giallongo et al. 1993, Cristiani et al. 1995) that the bulk of the line distribution lies in the b region between 20 and 30 km s^{-1} . There is a non-negligible fraction of lines with b in the range 10–20 km s^{-1} , 18% and 17% for 0000-26 and 2126-158 respectively, with very few cases ($\lesssim 2\%$) of lines with $b < 10 \text{ km s}^{-1}$, which

may be representative of unrecognized metal lines. Since the profile fitting of narrow lines with $\log N_{HI} < 13$ can be affected by systematic errors due to the present S/N (Rauch et al. 1993) we have computed the same fraction for lines with $\log N_{HI} \geq 13$ finding 16% and 15% in both spectra. In any case, the fraction of low- b lines appears to be uncorrelated with the S/N.

It is well known (e.g. Pettini et al. 1990, Donahue & Shull 1991) that Doppler b values corresponding to temperatures $T \lesssim 20000$ K are difficult to reconcile with sizes greater than 50 kpc. Giallongo & Petitjean 1994 emphasized the importance of inverse Compton cooling by the cosmic microwave background radiation and of a steepening of the ionizing background at wavelengths shorter than the HeII edge to get sufficient cooling rate to obtain temperatures as low as 18000 – 20000 K with sizes up to 100 – 200 kpc. In all these analyses both photoionization and thermal equilibrium were assumed, neglecting explicit time dependence of the photoionization mechanisms, which may be important at redshifts $z \gtrsim 3$.

Ferrara & Giallongo 1995 recently developed a time dependent photoionization code that follows the thermal history of the photoionized gas with total density $n_H \lesssim 10^{-4} \text{ cm}^{-3}$ out of the ionization and thermal equilibrium. They show that it is possible to get temperatures as low as 15000 K at $z > 3$ provided that the ionization starts at redshifts appreciably higher than 7 and that the UVB has a jump at the HeII edge by a factor of the order of 100. This corresponds to minimum Doppler values of the order of $b \sim 14 \text{ km s}^{-1}$, consistent with the minimum values observed in our sample. Thus, the existence of narrow lines in the Lyman- α population may become a sensitive tool to constrain the epoch of reionization and the shape of the UVB.

2.3. The HI column density distribution

The column density distribution of the lines in our extended sample at a distance larger than 8 Mpc from the QSOs is shown in Fig. 6, in which the line density has been normalized at $z = 3$.

A double power-law distribution clearly appears with a break at $\log N_{HI} = 14$. Below the break the slope is very flat ($\beta_f \sim 1.1$) down to our selection threshold $\log N_{HI} \simeq 13$. Above the break the slope is steep with $\beta_s \sim 1.8$. There are two main biases that do alter the shape of the column density distribution. Strong saturated lines above the break often show complex structures, but independently of the S/N, these features can not be deblended without information on the Lyman- β forest, which are often outside the observed range or heavily contaminated by lower- z Lyman- α lines.

The distribution of the lines below the break is affected by the so-called “line-blanketing” effect, due to high column density lines that conceal weak lines. In order to quantify and correct this effect, which becomes more and more important at higher redshifts, we have performed extensive simulations with the FITLYMAN code, trying to mimic the blanketing process. Each set of simulations was performed by progressively merging two lines (a “weak” and a “strong” line) of given parameters: fig. 7a shows an example at S/N=10. At each separation, a profile fit with a single component was attempted. We have defined the critical separation as the distance for which the fit turns out to be acceptable in the 50% of trials (about 0.7 \AA in this case, see fig. 7b). At smaller separations, with the assigned S/N ratio, resolution and redshift, the weak line is definitely lost. In Figs. 7c,d a similar simulation is shown for a line pair with larger b parameters. As expected, in this case the critical separation is larger, $\sim 1 \text{ \AA}$. This critical separation, which is a function of several parameters (the S/N ratio, the Doppler parameters of the lines and their column densities, the average absorption redshift and the resolution) was computed for a grid in the parameter space corresponding

to the available data. In this way we have been able to quantify the effects of the blanketing on the line selection function. Lines with $\log N_{HI} = 13.3 - 13.5$ are lost in the $\sim 35\%$ of the observed redshift interval at $z \simeq 4$, in the $\sim 17\%$ at $z \simeq 3$ and in the $\sim 11\%$ at $z \simeq 2$.

The effects of this correction on the column density distribution are shown in fig. 6 (dashed histogram), where the number density of the lines in the different column density bins has been normalized to the effective redshift range derived for each QSO spectrum. The change in slope is still present and well represented by a double power-law, although the average slope below the break is increased to $\beta_f \sim 1.4$, a value consistent with previous estimates obtained at lower redshifts (Giallongo et al. 1993, Cristiani et al. 1995) where line blanketing effects are less important. The corrected distribution has been computed down to $\log N_{HI} = 13.3$ which is the completeness threshold of our extended sample.

2.4. The Redshift Distribution

The observed number density of the extended sample of Lyman- α clouds with $\log N_{HI} \geq 14$ is plotted in Fig. 8 as a function of redshift together with that of the Lyman Limit and Damped systems recently derived by Storrie-Lombardi et al. 1994; 1995. The number density of Ly α clouds at $z < 1.7$ derived from the HST data of Bahcall et al. 1995 is also plotted.

Assuming a standard power-law evolution of the type $dn/dz \propto (1+z)^\gamma$, Storrie-Lombardi et al. found $\gamma = 1.5$ for both populations, while we find (see Section 3) $\gamma = 2.7$ for the Lyman- α clouds. Of course, the derived number densities span about two orders of magnitude.

Estimates of the comoving volume densities can be derived using information about the sizes of the different populations. Bechtold et al. 1994 give, assuming spherical geometry, a median value for the radius of Lyman- α clouds of the order of 200 kpc. The Lyman Limit population is virtually indistinguishable from the population selected by the presence

of MgII absorption which is found to be associated with the internal parts of the galaxy halos (Bergeron & Boissé 1991). From the statistics of the galaxies responsible for the MgII absorptions it is possible to derive an average radius of the order of 40 kpc (Steidel 1995).

For the damped systems, typical HI column densities $\geq 2 \times 10^{20} \text{ cm}^{-2}$ imply disks of ~ 20 kpc radii (Smette et al. 1995; Broeils & van Woerden 1994; Steidel et al. 1995). With such sizes and geometries the volume densities of the Lyman- α clouds with $\log N_{HI} \gtrsim 14$, i.e. at the break of the column density distribution, and of the Lyman Limit and Damped systems appear remarkably similar, as shown in Fig. 9. Also their cosmological evolutions appear consistent in the overall redshift range.

Thus, it is tempting to interpret the Lyman- α clouds with $\log N_{HI} \gtrsim 14$ as gas associated with the outer regions of the same class of galaxies responsible for the Lyman Limit and Damped systems.

A Lyman- α -galaxy association was originally proposed by Bahcall & Spitzer 1969 and it is now statistically suggested at low redshift by imaging of the galaxy-fields surrounding QSOs (Lanzetta et al. 1995).

A scenario of this kind is in agreement with the observations of metallicities of the order of 10^{-2} in the Lyman- α clouds (Cowie et al. 1995, Tytler & Fan 1995) and also with the detection of clustering of the Lyman- α clouds with $\log N_{HI} \gtrsim 14$ (Cristiani et al. 1995; Meiksin & Bouchet 1995).

The Lyman- α absorptions with $\log N_{HI} \lesssim 14$ (the flat part of the column density distribution), would be in part associated with galaxies and in part due to fluctuations of a clumpy intergalactic medium.

3. The measure of the UV Background from the proximity effect

We can parameterize the line distribution far away from the QSOs as a function of the column density and redshift:

$$\frac{\partial^2 n}{\partial z \partial N_{HI}} = A_o (1+z)^\gamma \begin{cases} N_{HI}^{-\beta_f} & N_{HI} < N_{break} \\ N_{HI}^{-\beta_s} N_{break}^{\beta_s - \beta_f} & N_{HI} \geq N_{break} \end{cases} \quad (1)$$

Near the QSO, highly ionized clouds are observed with a column density

$$N_{HI} = \frac{N_\infty}{1 + \omega} \quad (2)$$

i.e. the ratio between the intrinsic column density N_∞ , which the same cloud would have at infinite distance from the QSO, and the factor $1 + \omega$, where:

$$\omega(z) = \frac{F}{4\pi J} \quad (3)$$

is the ratio between the flux F that the cloud receives from the QSO and the flux J that the cloud receives from the general UVB (see Bajtlik et al. 1988 and Bechtold 1994 for details of the model).

Adopting the following conservation law near the QSO emission redshift we have

$$f(N) = g(N_\infty) dN_\infty / dN = g(N_\infty) (1 + \omega) \quad (4)$$

where $f(N)$ and $g(N_\infty)$ are the column density distributions near the QSO and at infinite distance.

We have used the following double power-law distribution to get a simultaneous estimate of the Lyman- α parameters of the N_{HI} , z distributions *and* of the UV background $J_{LL}(z)$ evaluated at the Lyman limit.

$$\frac{\partial^2 n}{\partial z \partial N_{HI}} = A_o (1+z)^\gamma (1+\omega)^{1-\beta_f} \begin{cases} N_{HI}^{-\beta_f} & N_{HI} < N_{break} \\ N_{HI}^{-\beta_s} N_{break}^{\beta_s - \beta_f} & N_{HI} \geq N_{break} \end{cases} \quad (5)$$

where

$$N_{break}(z) = \frac{N_{\infty,b}}{1 + \omega(z)}$$

is the observed break, which is shifted to lower and lower N_{HI} as the QSO emission redshift is approached,

It is clear from the previous equation that the measure of J depends critically on the estimates of β_f , because the bulk of the lines comes from this part of the distribution, and on γ . For this reason, it is not strictly correct to separate the analysis of the Lyman- α line distribution from the estimate of J , as done in previous analyses performed at lower resolution, and a Maximum Likelihood Analysis which adopts the line distribution given in Eq. 5 has to be used.

A similar approach has been adopted by Kulkarni and Fall 1993 using low redshifts HST spectra. However, their data are at low resolution and they derived column densities from a curve of growth analysis assuming an average Doppler parameter for all the lines and a single power-law N_{HI} distribution.

In Table 2 we have reported the result of the ML analysis. The redshift evolution is confirmed at about the same level previously found at lower resolution (e.g Lu, Wolfe & Turnshek 1991, Bechtold 1994). The column density distribution is well represented by a double power-law, as already shown in Fig. 6, with a very flat slope below the break at $\log N_{HI} \sim 14$. Another important result concerns the UV background derived from the proximity effect that appears definitely smaller than previously reported, i.e. $J_{-22} = 6 \pm 1$ in the redshift interval $z = 1.7 - 4.1$.

The redshifts adopted in Table 1 are derived from low ionization lines (OI, MgII, H α), which are representative of the true systemic redshift of the QSO (Gaskell 1982, Espey et al. 1989). Using high ionization lines (e.g. CIV, SiIV etc.), which typically provide a smaller redshift, would result in an overestimate of the value of the UV background derived from

the proximity effect by a factor of ~ 2 (Espey 1993, Bechtold 1994).

As apparent in equation 5, the value of J is sensitive to the precise value of β_f . Thus, it is important to apply a blanketing correction below the break of the column density distribution. To this end, we have introduced for each spectrum in the Maximum Likelihood Analysis an effective redshift range which is a function of column density and redshift, as defined in the section 2.3.

The result is shown in Table 3: the correction for the blanketing effects increases the rate of the redshift evolution and steepens the column density distribution below the break. Because of these changes, the intrinsic number density of lines far away from the QSOs increases especially at high redshifts, and this in turn causes a decrement of the value of the UV background derived from the proximity effect down to $J_{-22} = 5 \pm 1$.

We have repeated the ML analysis allowing for a power-law redshift evolution of the UVB of the kind

$$J = J_{(z=3)} \left(\frac{1+z}{4} \right)^j \quad (6)$$

The best fit slope j shown in Table 3 is negative but consistent with no evolution in the redshift interval $z = 2 - 4$, although the uncertainties are still large.

The present statistical analysis, based on the ML formalism, allows an accurate measure of the UV background, even if systematic biases could be present. Bechtold 1994 gave a comprehensive discussion of the various systematic errors possibly affecting any estimate of the UVB. One of the main source of errors concerns the assumption of the same spectral shape for the UVB and the spectrum of the individual QSOs, which is implicit in the Bajtlik et al. 1988 model. Bechtold 1994, comparing the ionization rate due to an UVB produced by QSOs alone with the one produced by the sum of QSOs and primeval galaxies, estimated small changes ($\lesssim 25\%$) in the ratio of the ionization rates.

Recent measurements of HeII Lyman- α absorption in QSO spectra (Jakobsen et al. 1994, Davidsen et al. 1995) show that a strong decrease, i.e. a “jump” by a factor $\sim 70-100$, in the shape of the UVB should be present just above the HeII edge (4 Rydberg). However, detailed Lyman- α photoionization models by Ferrara & Giallongo 1995 show that, even in this case, no appreciable changes in the hydrogen ionization fractions are present either including or excluding the jump in the spectral shape of the UV background. Thus the assumption of the simple power-law shape adopted in this paper and in Bechtold 1994 remains a valid approximation.

Other biases such as magnification by gravitational lensing could be present for some QSOs, but the statistical effect is expected to be small (Bechtold 1994), on the ground of the correlation of the proximity effect with luminosity and not with redshift.

QSO variability on a time scale of the order of the photoionization time ($\sim 10^4$ yr) could also affect the estimate of the proximity effect, but the result should simply be an increase in the statistical variance of our measure without changing the average value.

The value of J so derived is a factor of 6 lower than previous estimates (e.g. Bechtold 1994) from data at low resolution using the same simple model. This difference can be ascribed essentially to the assumption of a single power-law distribution with the canonical slope -1.7 adopted by Bechtold 1994 and to the blanketing effects which are stronger at low resolution.

The new value we have found is remarkably close to the one predicted for the integrated contribution of QSOs, in particular once dust obscuration of the QSO population (Meiksin & Madau 1993; Fall & Pei 1995) is taken into account.

Following the line of argument described in Giallongo et al. 1994, we can use the 5 ± 1 value of J_{22} together with the $\tau < 0.05$ 1σ upper limit for the GP optical depth at $z \sim 4.5$,

to derive a value for the density of the diffuse part of the intergalactic medium, which turns out to be rather low, $\Omega_{IGM} \lesssim 0.01$.

4. Conclusions

A sample of absorption lines has been extracted from the spectra of 6 QSOs taken at an average resolution of 11 km s^{-1} over the absorption redshift range $z = 2.8 - 4.1$. Merging these data with those of 4 other QSOs with observations of similar quality available in the literature has provided a relatively large Lyman- α sample (more than 1100 lines), to which a Maximum Likelihood analysis has been applied to estimate simultaneously the best fit parameters of the Lyman- α clouds statistics and the intensity of the UVB background in the redshift interval $z = 1.7 - 4.1$.

The main results of our study are:

1. From the subsample of Lyman- α lines from the spectra at higher S/N we derive, in the range $z = 3 - 4$, a typical Doppler parameter in the range $b = 20 \div 30 \text{ km s}^{-1}$ and estimate a fraction $\sim 15 - 18\%$ of lines with $10 \leq b \leq 20 \text{ km s}^{-1}$, corresponding to average temperatures $T \sim 15000 \text{ K}$, still consistent with models of low density, highly ionized clouds .
2. We confirm the presence of a break in the column density distribution at $\log N_{HI} = 14$ with a flat slope $\beta_f \simeq 1.4$ for the lower column densities and a steep one, $\beta_s \simeq 1.8$, for the higher column densities.
3. An interesting similarity is revealed between the volume density distributions of Lyman Limit systems, Damped systems and Lyman- α clouds, as derived on the basis of their estimated sizes and geometries. This suggests a physical association between the Lyman- α clouds with $\log N_{HI} \gtrsim 14$ and the halos of protogalactic systems.

4. The intensity of the UV background J as derived from the proximity effect is a factor of 6 lower than previously estimated, with the same photoionization model, from data at lower resolution, for which the blanketing effects are stronger. The value $J_{-22} \simeq 5 \pm 1$ we have found is consistent with the one predicted for QSOs after allowing for some dust obscuration of the QSO population.
5. No evidence is found, within relatively large uncertainties, for evolution in redshift of the UVB in the range $z = 1.7 - 4.1$.

We thank K. Lanzetta, L. Lu and P. Madau for useful discussions.

Table 1
QSO Spectra from the ESO KP

QSO Name	z_{min}	z_{em}	FWHM (km s ⁻¹)	Mag
2126 – 15	2.51	3.27	11	V=17.3
2355 + 01	3.12	3.39	9	V=17.5
0055 – 26	2.96	3.67	14	V=17.5
1208 + 10	3.57	3.82	9	V=17.5
1108 – 07	3.72	3.95	9	R=18.1
0000 – 26	3.60	4.12	12	V=17.5

Other QSO Spectra

QSO Name	z_{min}	z_{em}	FWHM (km s ⁻¹)	Mag
1331 + 17 ^a	1.68	2.10	18	V=16.9
1101 – 26 ^b	1.84	2.15	9	V=16.0
2206 – 19 ^c	2.09	2.56	6	V=17.3
0014 + 81 ^d	2.70	3.41	23	V=16.5

References: ^a Kulkarni et al. 1995, ^b Carswell et al. 1991, ^c Rauch et al. 1993, ^d Rauch et al. 1992

Table 2

Maximum likelihood analysis for lines with $\log N_{HI} \geq 13.3$

N_l	γ	β_f	$\log N_{\infty,b}$	β_s	J
1128	2.49 ± 0.21	1.10 ± 0.07	14.00 ± 0.02	1.80 ± 0.03	-21.21 ± 0.07

Table 3

Maximum likelihood analysis for lines with $\log N_{HI} \geq 13.3$
with blanketing corrections

γ	β_f	$\log N_{\infty,b}$	β_s	J	j
2.65 ± 0.21	1.35 ± 0.07	13.98 ± 0.04	1.80 ± 0.03	-21.32 ± 0.08	-
2.67 ± 0.26	1.34 ± 0.09	13.96 ± 0.07	1.80 ± 0.04	-21.32 ± 0.10	-0.28 ± 1.41

REFERENCES

- Bahcall, J. N. 1968, ApJ, 153, 679
- Bahcall, J. N. et al. 1995, ApJ, in press
- Bahcall, J. N., & Spitzer, L. 1969, ApJ, 156, L63
- Bajtlik, S., Duncan, R. C., & Ostriker, J. P. 1988, ApJ, 327, 570
- Bechtold, J. 1994, ApJS, 91, 1
- Bechtold, J., Crofts, A. P. S., Duncan, R. C., & Fang, Y. 1994, ApJ, 437, L83
- Bergeron, J., & Boissé, P. 1991, A&A, 243, 344
- Broeils, A. H., & van Woerden, H. 1994, A&AS, 107, 129
- Carswell, R. F., Lanzetta, K. M., Parnell, H. C., & Webb, J. K. 1991, ApJ, 371, 36
- Cen, R., Miralda-Escudé, J., Ostriker, J. P., & Rauch, M. 1994, ApJ, 437, L9
- Cristiani, S., D’Odorico, S., Fontana, A., Giallongo, E., & Savaglio, S. 1995, MNRAS, 273, 1016
- Cowie, L. L., Songaila, A., Kim, T., & Hu, E. M., 1995, AJ, 109, 1522
- Davidson, A. F., Kriss, G. A., & Zheng, W. 1995, Nature, submitted
- Dinshaw, N., Foltz, C. B., Impey, C. D., Weymann, R. J., & Morris, S. L. 1995, Nature, 373, 223
- Donahue, J. M., & Shull, J. M. 1991, ApJ, 383, 511
- Espey, B. R. 1993, ApJ, 411, L59
- Espey, B. R., Carswell, R. F., Bailey, J. A., Smith, M. G., & Ward, M. J. 1989, ApJ, 342, 666
- Fall, M., & Pei, Y. C. 1995, to appear in the *Proceedings of the ESO Workshop on QSO Absorption Lines*, ed. G. Meylan (Berlin: Springer-Verlag)

- Fan, X.–M., Tytler, D. 1994, *ApJS*, 94, 17
- Ferrara, A., & Giallongo, E. 1995, in preparation
- Fontana, A., Ballester, P. 1995, *The Messenger*, 80, 37
- Gaskell, C. M. 1982, *ApJ*, 263, 79
- Giallongo, E., Cristiani, S., Fontana, A., Trevese, D. 1993, *ApJ*, 416, 137
- Giallongo, E., D’Odorico, S., Fontana, A., McMahon, R. G., Savaglio, S., Cristiani, S., Molaro, P., Trevese, D. 1994, *ApJ*, 425, L1
- Giallongo, E., Petitjean, P., 1994, *ApJ*, 426, L61
- Jakobsen, P., Boksenberg, A., Deharveng, J. M., Greenfield, P., Jedrzejewski, R., & Paresce, F. 1994, *Nature*, 370, 35
- Kulkarni, V. P., & Fall, S. M. 1993, *ApJ*, 413, L63
- Kulkarni, V. P., Huang, K., Green, R. F., Bechtold, J., Welty, D. E., & York D. G. 1995, *MNRAS*, submitted
- Lanzetta, K. M., Bowen, D. B., Tytler, D., & Webb, J. K. 1995, *ApJ*, 442, 538
- Lu, L., Wolfe, A. M., & Turnshek, D. A. 1991, *ApJ*, 367, 19
- Meiksin, A, & Bouchet, R. F. 1995, *ApJ*, 448, L85
- Meiksin, A., & Madau, P. 1993, *ApJ*, 412, 34
- Miralda–Escudé, J., & Rees, M. J. 1994, *MNRAS*, 266, 343
- Morton, D. C. 1991, *ApJS*, 77, 119
- Pettini, M., Hunstead, R. W., Smith, L. J., & Mar, D. P. 1990, *MNRAS*, 246, 545
- Rauch, M., Carswell, R. F., Chaffee, F. H., Foltz, C. B., Webb, J. K., Weymann, R. J., Bechtold, J., & Green, R. F. 1992, *ApJ*, 390, 387
- Rauch, M., Carswell, R. F., Webb, J. K., & Weymann, R. J. 1993, *MNRAS*, 260, 589

- Smette, A., Robertson, J. G., Shaver, P. A., Reimers, D., Wisotzki, L., & Kohler, Th. 1995, A&A, in press
- Smette, A., Surdej, J., Shaver, P. A., Foltz, C. B., Chaffee, F. H., Weymann, R. J., Williams, R. E., & Magain, P. 1992, ApJ, 389, 39
- Steidel, C. C. in the *Proceedings of the ESO Workshop on QSO Absorption Lines*, ed. G. Meylan (Berlin: Springer-Verlag), p. 139
- Steidel, C.C., Bowen, D.V., Blades, J.C., & Dickinson, M. 1995, ApJ, 440, L45
- Storrie-Lombardi, L. J., McMahon, R. G., Irwin, M. J., & Hazard, C. 1994, ApJ, 427, L13
- Storrie-Lombardi, L. J., McMahon, R. G., Irwin, M. J., & Hazard, C. 1995, in the *Proceedings of the ESO Workshop on QSO Absorption Lines*, ed. G. Meylan (Berlin: Springer-Verlag) p. 47
- Tytler, D. 1987, ApJ, 321, 49
- Tytler, D. & Fan, X–M. 1995, submitted to ApJ
- Weymann, R. J., Carswell, R. F., & Smith M. G. 1981, ARA&A, 19, 41

FIGURE CAPTIONS

Fig. 1. Examples of fits in the Lyman- α forest together with the corresponding Lyman- β forest.

Fig. 2. Normalized spectra of the regions near the Lyman- α emissions for PKS 2126-158 (upper plots) and Q0000-26 (lower plots). The dashed line shows the noise level per resolution element.

Fig. 3. Doppler parameter - column density plane for the lines out of 8 Mpc from the QSO 0000-26.

Fig. 4. Doppler parameter - column density plane for the lines out of 8 Mpc from the QSO 2126-158.

Fig. 5. Doppler distributions of the lines shown in Figs. 3 and 4(continuous histogram for 0000-26).

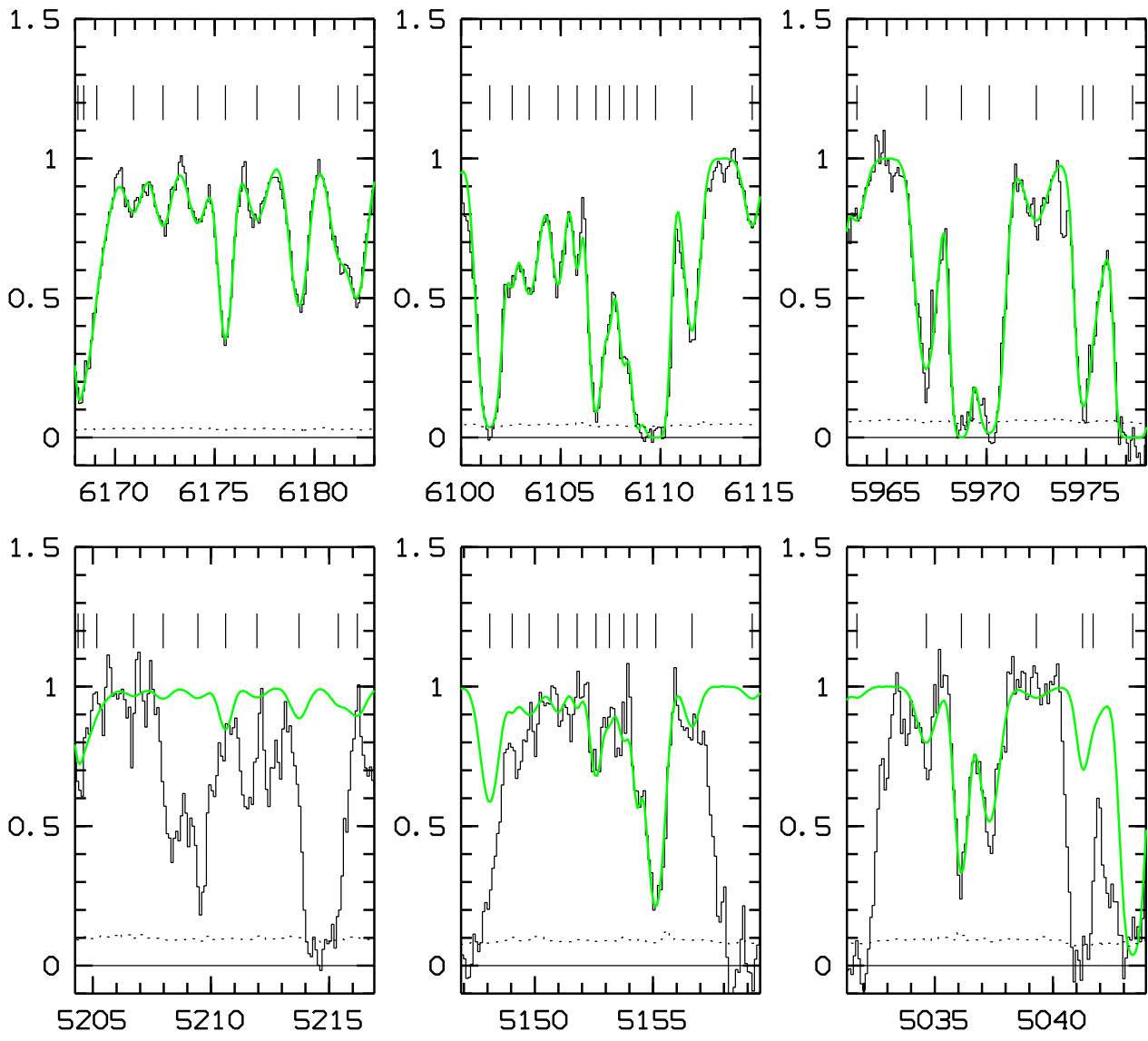
Fig. 6. Column density distribution for the overall composite sample (continuous histogram). The dashed part shows the blanketing correction.

Fig. 7. a,c) Blanketing simulation for line pairs. b,d) Fraction of acceptable fits ($P > 0.05$) with a single line as a function of the separation of the line pair.

Fig. 8. Redshift distribution of the Lyman- α lines with $\log N_{HI} \geq 14$. At $z < 1.7$ the number density of the low resolution HST sample is shown for lines with equivalent width $W \geq 0.28 \text{ \AA}$. The minimum value corresponds to $\log N_{HI} \simeq 14$ for $b = 30 \text{ km s}^{-1}$ as adopted

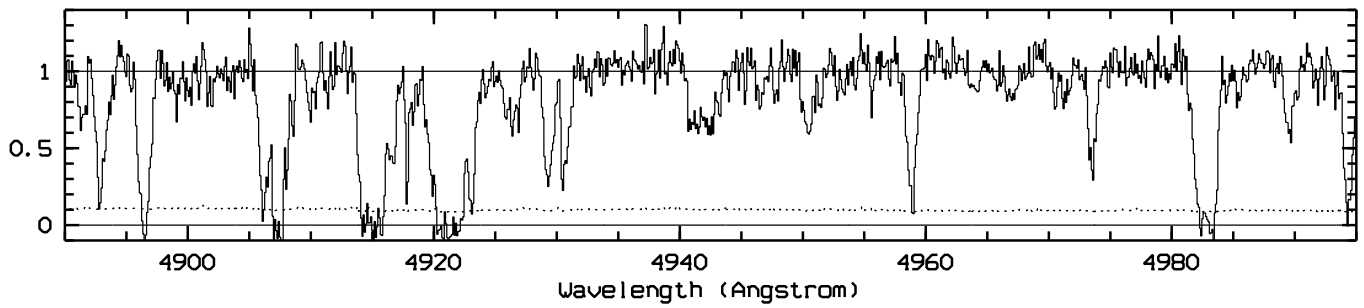
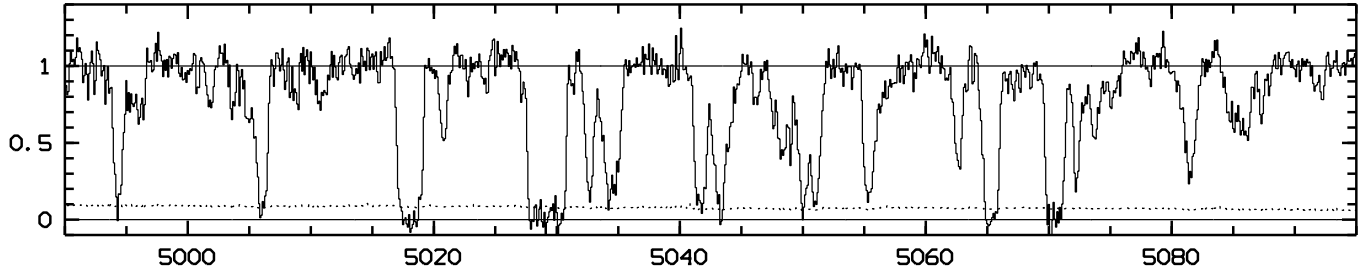
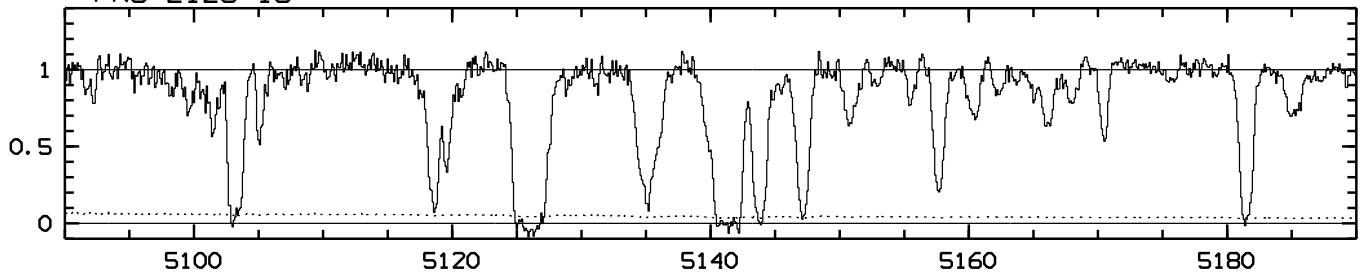
in our high resolution sample. The redshift distribution of the damped systems is also shown by the thick points and that of the Lyman Limit systems by the dashed points.

Fig. 9. Comoving volume density of the same samples as in Fig. 8.



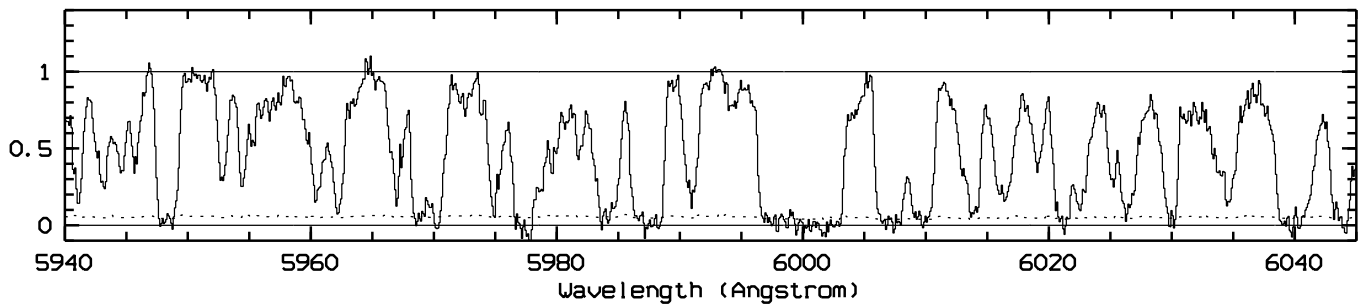
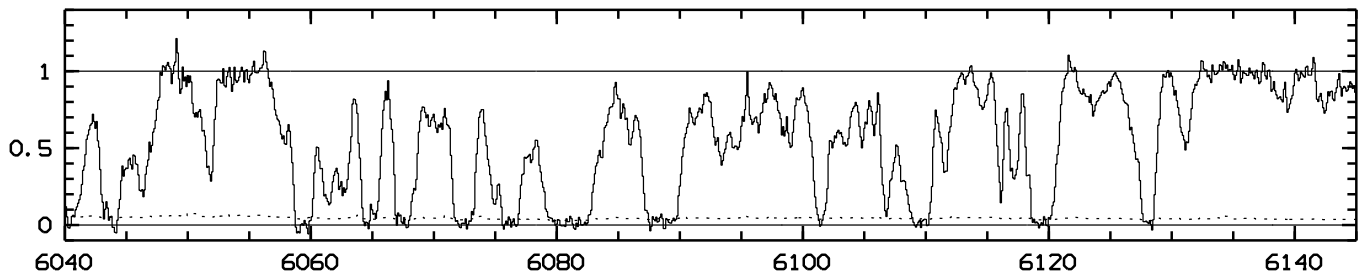
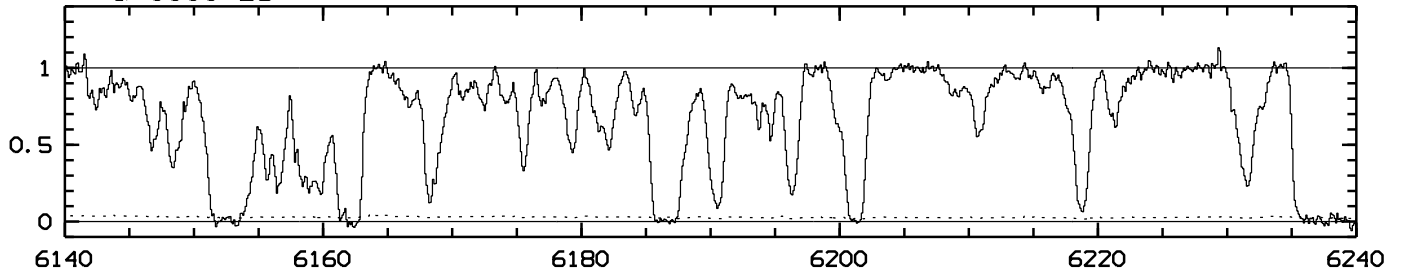
Wavelength (Angstrom)

PKS 2126-15



Wavelength (Angstrom)

Q 0000-26



Wavelength (Angstrom)

